

# Anomalous Spin-Wave Relaxation in Diluted Magnetic Semiconductors

J. E. Bunder,<sup>1</sup> Shih-Jye Sun,<sup>2</sup> and Hsiu-Hau Lin<sup>1,3</sup>

<sup>1</sup>*Physics Division, National Center for Theoretical Sciences, Hsinchu 300, Taiwan*

<sup>2</sup>*Department of Applied Physics, National University of Kaoshung, Kaoshung 800, Taiwan*

<sup>3</sup>*Department of Physics, National Tsing-Hua University, Hsinchu 300, Taiwan*

(Dated: February 8, 2020)

We study a diluted magnetic semiconductor at finite temperature by developing a self-consistent Green's function approach, which treats thermal fluctuations, spin-wave excitations, spin kinematics and disorder on an equal footing. One of the unique features of this approach is that the thermal evolution of the spin-wave relaxation can be analyzed by computing the imaginary part of the Green's functions. Our numerics show that the spin-wave spectral function sharpens dramatically near the critical regime, indicating the ferromagnetic phase transition is not driven by the competition between exchange energy and thermal entropy as in Heisenberg-like models. Finally, we discuss the implications of the temperature-dependent relaxation for experimental observations.

PACS numbers: 75.40.Gb, 75.50.Dd, 76.50.+g

Information processing and data storage are the corner stones of modern computing. Recent developments in diluted magnetic semiconductors (DMS), such as doping III-V GaAs semiconductors with the transition metal Mn, have increased the possibility of merging these two key functions in one single material[1, 2]. The ferromagnetic phase, involving both localized and itinerant spins, can be explained by the RKKY-type exchange[3, 4, 5, 6, 7] mediated by itinerant holes in the diffusive regime. Near the insulating regime, an alternative mechanism invoking percolation of magnetic clusters[8] is at work.

In a recent paper[9], Priour, Hwang and Das Sarma integrated out the itinerant carriers and proposed a Heisenberg-like lattice model that treats disorder and thermal fluctuations on equal footing, which gave quantitative agreement with experimental data successfully. It is worth noting that, in their approach and other studies in the literature, the thermal fluctuations were treated within Weiss mean-field approximation and the spin-wave fluctuations were ignored. In this Letter, we develop a self-consistent Green's function approach that successfully combines both the Heisenberg lattice model and spin-wave theory. In addition, the Green's functions allow us to numerically compute the spin spectral function (see Fig. 1). Note that, in the Heisenberg model, the spin-wave relaxation is expected to increase smoothly as thermal fluctuations grow. In sharp contrast, when both itinerant and localized spins are retained and treated self-consistently, the width of the spectral function, i.e. the relaxation rate of the spin waves, actually sharpens when approaching the critical temperature!

To study the temperature dependence of the spin-wave relaxation, we begin with the simplest model[10],

$$H = H_0 + J \int d^3r \mathbf{S}(r) \cdot \boldsymbol{\sigma}(r), \quad (1)$$

where  $J > 0$  describes the antiferromagnetic exchange coupling between itinerant and localized spin densities

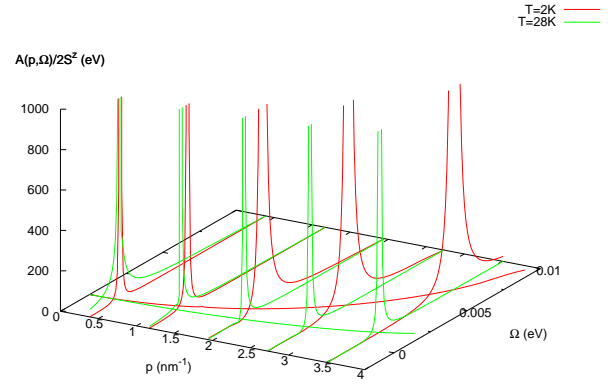


FIG. 1: (Color Online) Spin spectral function  $A(p, \Omega)/(2\langle S^z \rangle)$  at temperatures  $T = 2, 28K$  with density ratio  $n_h/n_I = 0.3$ .

and  $H_0$  is the kinetic energy of itinerant carriers with parabolic band  $\epsilon_p = \frac{p^2}{2m^*}$ . The impurity spin density is the sum over all randomly located impurity spins  $\mathbf{S}(r) = \sum_I \delta^3(r - R_I) \mathbf{S}_I$  and the itinerant spin density is defined by  $\boldsymbol{\sigma}(r) = \psi_\alpha^\dagger(r) (\boldsymbol{\sigma}/2)_{\alpha\beta} \psi_\beta(r)$ . We vary the density ratio of itinerant to impurity spins  $n_h/n_I$  but fix the exchange coupling  $J = 0.15 \text{ eV nm}^3$ [1] and the density of impurity spins  $n_I = 1 \text{ nm}^{-3}$  in all calculations.

We now introduce several Green's functions and compute them self-consistently. We emphasize that rather than treating the spin waves as bosons, the Green's function approach respects the spin kinematics which, as Dyson pointed out, is crucially important. The thermal Green's function for the impurity spins is defined by

$$\begin{aligned} iD(r_1, r_2; t) &\equiv i\langle\langle S^+(r_1, t); S^-(r_2, 0) \rangle\rangle \quad (2) \\ &= \theta(t)\langle S^+(r_1, t)S^-(r_2, 0) \rangle + \theta(-t)\langle S^-(r_2, 0)S^+(r_1, t) \rangle. \end{aligned}$$

To complete the self-consistency, it is necessary to introduce another Green's function which describes the corre-

lation between impurity and itinerant spins,

$$F(r_1, r'_1, r_2; t) \equiv \langle\langle \psi_\uparrow^\dagger(r_1, t) \psi_\downarrow(r'_1, t); S^-(r_2, 0) \rangle\rangle. \quad (3)$$

Using Heisenberg's picture, the dynamical equations for the Green's functions are

$$i\partial_t D(r_1, r_2; t) = 2\langle S^z(r_1) \rangle \delta(t) \delta^3(r_1 - r_2) - J\langle \sigma^z(r_1) \rangle D(r_1, r_2; t) + J\langle S^z(r_1) \rangle F(r_1, r_1, r_2; t), \quad (4)$$

$$\begin{aligned} i\partial_t F(r_1, r'_1, r_2; t) &= \left( \frac{\nabla_{r_1}^2}{2m^*} - \frac{J}{2} \langle S^z(r_1) \rangle \right) F(r_1, r'_1, r_2; t) - \frac{J}{2} \langle \psi_\downarrow^\dagger(r_1) \psi_\downarrow(r'_1) \rangle D(r_1, r_2; t) \\ &\quad - \left( \frac{\nabla_{r'_1}^2}{2m^*} + \frac{J}{2} \langle S^z(r'_1) \rangle \right) F(r_1, r'_1, r_2; t) + \frac{J}{2} \langle \psi_\uparrow^\dagger(r_1) \psi_\uparrow(r'_1) \rangle D(r'_1, r_2; t), \end{aligned} \quad (5)$$

where we take, for example  $\langle \sigma^z(r_1) S^+(r_1, t) S^-(r_2, 0) \rangle \approx \langle \sigma^z(r_1) \rangle \langle S^+(r_1, t) S^-(r_2, 0) \rangle$ . After changing variables  $D(r_1, r_2; t) = D(r, \Delta r; t)$  followed by Fourier transformation to  $D(r, p; \Omega)$ , the position-dependent dispersion of the spin wave  $\omega_p(r)$  can be found by looking for poles of the Green's function  $D^{-1}(r, p; \omega_p) = 0$ , where  $r \equiv (r_1 + r_2)/2$ ,  $\Delta r \equiv r_1 - r_2$  and  $p$  is the conjugate momentum of  $\Delta r$ . To complete the self-consistent loop, we need to determine the expectation values of all terms in the coupled differential equations. We may generalize Callen's formula[11] to evaluate the polarization of the impurity spins,

$$\frac{\langle S^z(r) \rangle}{n_I} = S - \langle n_{sw} \rangle + \frac{(2S+1)\langle n_{sw} \rangle^{2S+1}}{(1+\langle n_{sw} \rangle)^{2S+1} - \langle n_{sw} \rangle^{2S+1}}. \quad (6)$$

where the average number of spin waves is  $\langle n_{sw} \rangle = (1/n_I) \int d^3k / (2\pi)^3 [e^{\beta\omega_k(r)} - 1]^{-1}$ . The difference between the independent spin-wave theory and the self-consistent Green's function method lies in the third term, which correctly accounts for the spin kinematics.

The polarization of impurity spins  $\langle S^z(r) \rangle$  gives rise to a Zeeman splitting of the itinerant carriers and thus a finite polarization  $\langle \sigma^z(r) \rangle$ . Similarly, the correlators  $\langle \psi_\alpha^\dagger(r) \psi_\alpha(r') \rangle$  can be computed from the Zeeman splitting. Finally, the coupled Green's functions  $D(r_1, r_2; t)$  and  $F(r_1, r'_1, r_2; t)$ , which are capable of handling the spatial inhomogeneities due to randomly located impurity spins, the spatial and thermal fluctuations of spin waves at finite temperatures and also the non-trivial spin-wave kinematics, can be solved self-consistently by numerical methods. To the best of our knowledge, this is the only scheme which is capable of simultaneously incorporating all these effects.

Solving the coupled differential Eqs. (4) and (5) is not a trivial numerical task, although, some simplifications can be made when the density ratio  $n_h/n_I$  is small, so that the Fermi wavelength is much larger than the average distance between impurity spins. In the diffusive regime, after a coarse-graining procedure, the

translational invariance is approximately restored and the Green's functions are only functions of the relative distance. This approximation is justified by recent numerical calculations[12] which found that magnetization curves with different disorder configurations are almost identical. Thus, in the regime  $n_h/n_I \ll 1$ , even though the disorder may play a role in the pursuit of quantitative precision, it is not essential for the qualitative descriptions we desire here.

The restoration of translational symmetry simplifies the solution of the coupled differential equations. In the Fourier space, Eq. (5) simplifies to  $F(k, k+p; \Omega) = G(k, k+p; \Omega)D(p, \Omega)$  with

$$G(k, k+p; \Omega) = \frac{Jn_h}{2} \frac{f_\uparrow(\epsilon_k) - f_\downarrow(\epsilon_{k+p})}{\Omega + \epsilon_k - \epsilon_{k+p} + \Delta + i\gamma_h}, \quad (7)$$

where  $f_\alpha(\epsilon_k) = [e^{\beta(\epsilon_k + \alpha\Delta/2 - \mu)} - 1]^{-1}$  is Fermi distribution for itinerant carriers with the Zeeman gap  $\Delta = J\langle S_z \rangle$ . Positive, finite  $\gamma_h$  is introduced for numerical convergence and can be used to provide a phenomenological description of the relaxation rate of itinerant spins. On substituting the expression for  $F(k, k+p; \Omega)$  into Eq. (4), the spin-wave propagator is solved,

$$D(p, \Omega) = \frac{2\langle S_z \rangle}{\Omega + \Sigma(p, \Omega) + i\gamma_I}, \quad (8)$$

where the prefactor  $2\langle S^z \rangle$  arises from the exact treatment of spin-wave kinematics and a bare relaxation rate for the impurity spins  $\gamma_I$  is introduced for numerical convergence. On phenomenological grounds, we expect  $\gamma_I \ll \gamma_h$  and therefore, in Eq. (8) the impurity relaxation rate is negligible compared to the self-energy  $\Sigma(p, \Omega)$  of interactions between itinerant and impurity spin densities which consists of two terms

$$\Sigma(p, \Omega) = J\langle \sigma^z \rangle - \frac{\Delta}{n_h} \int \frac{d^3k}{(2\pi)^3} G(k, k+p; \Omega). \quad (9)$$

The first term coincides with the conventional Weiss mean-field theory approach but, the second term is vitally important in describing the spin-wave relaxation.

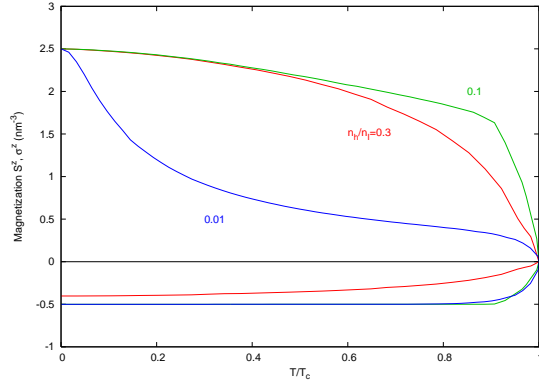


FIG. 2: (Color Online) The magnetization curves of impurity and itinerant spins at different density ratios  $n_h/n_I$ .

Because the first term is always real, dropping the second term would lose all information about the Landau damping of the spin waves inside the Stoner continuum, described by the imaginary part of the self-energy  $\Sigma_I(p, \Omega)$ .

From our numerical calculations,  $\Sigma_I$  is small and the spin-wave dispersion  $\omega_p$  is determined from the real part of the self-energy satisfying  $\omega_p + \Sigma_R(p, \omega_p) = 0$ . In general, when calculating the spin-wave dispersion, we find two poles which correspond to the gapless spin-wave excitations and the hybridization mode within the electronic Stoner continuum. Since the self-energy is analytic and the singularity of the Green's function is isolated, the meromorphic theorem gives

$$D(p, \Omega) = 2\langle S^z \rangle \sum_{i=1,2} \frac{Z_i}{(\Omega - \omega_p^i) + i\Gamma_i} + C, \quad (10)$$

where  $C$  is some constant. The dispersion and relaxation rate for each mode are  $\omega_p^i$  and  $\Gamma_i$  respectively. The spectral weight for each mode is  $Z_i$  which satisfies the sum rule  $Z_1 + Z_2 = 1$ . For small density ratios  $n_h/n_I$ , the spectral weight of the hybridization mode is negligible,  $Z_2 \ll Z_1$ , so we just consider frequencies close to the gapless mode  $\Omega \sim \omega_p^1$  and ignore the contribution from the hybridization mode.

Therefore, for a given set of itinerant and impurity spin configurations  $\langle \sigma^z \rangle$  and  $\langle S^z \rangle$ , the spin-wave dispersion  $\omega_p$  may be evaluated numerically (we drop the superscript for clarity). Making use of the Callen's formula in Eq. (6), we may self-consistently evaluate  $\langle \sigma^z \rangle$ ,  $\langle S^z \rangle$  and  $\omega_p$ . Numerically, we start with the configuration calculated for the previous temperature step and iterate the self-consistent procedure until a convergence is reached. The magnetization curves for different density ratios  $n_h/n_I$  are shown in Fig. 2. While this is not the main focus of our results, we emphasize the sensitivity in the shape of the magnetization curve to the density ratio. In particular, for density ratio  $n_h/n_I = 0.1$ , the magnetization curve decreases linearly with a very small gradient and, only in the narrow regime near the critical tempera-

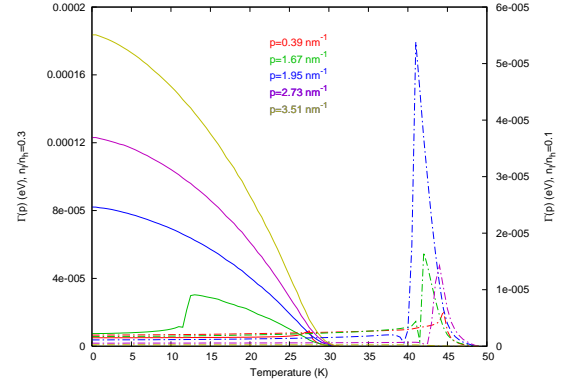


FIG. 3: (Color Online) Spin-wave relaxation rate  $\Gamma(p)$  at different momenta and density ratios  $n_h/n_I = 0.3, 0.1$ . The bare spin relaxation rate is chosen to be  $\gamma_h = 1 \times 10^{-4}$  eV. The solid (broken) lines correspond to the left (right) axis.

ture, the magnetization dives to zero and the phase transition occurs. Similar magnetization curves have been observed in some experiments[13]. This behavior is quite different to what we expect for a Heisenberg-like model where the phase transition is driven by a competition between exchange energy and thermal entropy. It is unlikely that the entropy gains would increase so drastically within such a short temperature interval and drive the phase transition to a paramagnetic state. In fact, as will be discussed, we find a peak in the spin relaxation which corresponds to the sudden decline in the magnetization.

The unique feature of the Green's function approach is that we can also study the temperature evolution of the spin spectral function as shown in Fig. 1. From Eq. (10), the imaginary part of the spin-wave propagator takes the Lorentzian form,

$$\begin{aligned} A(p, \omega) &= -\left(\frac{1}{\pi}\right) \text{Im}D(p, \Omega), \\ &= 2\langle S^z \rangle \left(\frac{Z}{\pi}\right) \frac{\Gamma(p)}{(\Omega - \omega_p)^2 + \Gamma(p)^2}. \end{aligned} \quad (11)$$

Note that the relaxation rate of the spin waves  $\Gamma(p) \approx \Sigma_I(\omega_p)$ , which can be shown after a Taylor expansion of the imaginary part of the self-energy  $\Sigma_I(p, \Omega)$  in the vicinity of  $\Omega \sim \omega_p$ . The temperature-dependent relaxation rates of spin waves with  $n_h/n_I = 0.3, 0.1$  are shown in Fig. 3. One may naively expect increasing thermal fluctuations to increase the relaxation rate, but our numerical results show the opposite trend. As the critical temperature is approached, the life time of the spin wave diverges, as is clearly seen for the density ratio  $n_h/n_I = 0.3$ . This peculiar phenomena indicates that the entanglement between the spin wave and the electronic magnons in the Stoner continuum is weaken when the phase transition is approached. It indicates that the ferromagnetic phase transition occurs because the impurity spins gradually become quasi-free and the magnetization

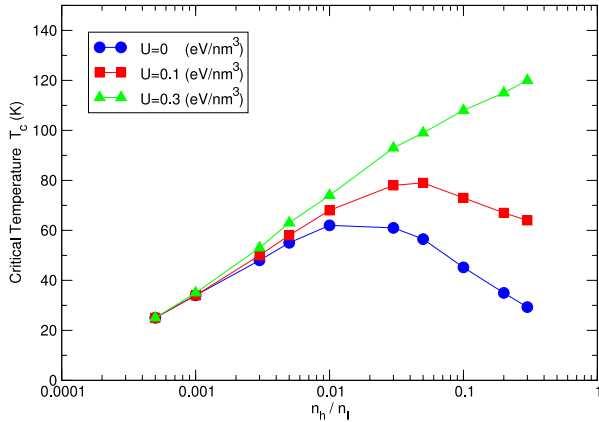


FIG. 4: (Color Online) Trends of the critical temperatures versus density ratio  $n_h/n_I$  with different on-site interaction strength  $U = 0, 0.1, 0.3 \text{ eVnm}^{-3}$ .

disappears. This underlying mechanism is drastically different from the conventional Heisenberg-like model where the phase transition is a direct consequence of competition between exchange energy and entropy.

In addition to the general trend of vanishing relaxation as the critical temperature is approached, for smaller density ratios such as  $n_h/n_I = 0.1$ , a peak structure appears in the vicinity of the phase transition. A sharp peak in the relaxation rate indicates the interactions between spin waves and electronic magnons (in the Stoner continuum) are enhanced and this should strongly affect the resistance. A naive consideration of Fermi's Golden rule implies that a peak in the relaxation rate near the critical temperature should produce a similar feature in the resistivity. Our finding agree with the peculiar resistance peak close to the critical point observed in as-grown samples[14], but more work needs to be done to establish the exact connection between peak structures in spin-wave relaxation and resistance.

Apparently, the existence of the peak structure is sensitive to the density ratio  $n_h/n_I$  and seems to be associated with the shape of the magnetization curve. In many as-grown DMS samples[15], the magnetization curves exhibit the peculiar linear-then-sharp-drop shape and a clear peak in resistance measurement. After annealing, the magnetization adopts a more conventional shape, accompanied by the disappearance of the resistance peak. Since annealing increases the density ratio, our numerical results describe the same trend as the experiments, i.e., the spin relaxation peak disappears when the density ratio is increased from  $n_h/n_I = 0.1$  to 0.3.

We now turn to open questions which were not considered in our calculations. Firstly, due to the advances in experimental techniques[15], it is now possible to fabricate DMS samples with  $n_h/n_I \sim 1$  where the ensemble average approximation may fail. In this limit, solving the coupled Green's functions self-consistently is more diffi-

cult than the numerical method we presented here. However, it is likely that the peak structure in the spin-wave relaxation, which vanishes as the density ratio increases for  $n_h/n_I < 1$ , will continue this trend for larger density ratios. Another issue is the implementation of a realistic band structure. From previous studies, we know that the *quantitative* description relies crucially on the correct band structure. However, qualitative features (such as the phase diagram) are already captured within the single-band model. Thus, we believe the results obtained here will survive the inclusion of a multi-band structure, but the dependence of various parameters is expected to be strongly renormalized. The electronic correlation can be easily included within the Green's function approach,

$$H_U = U \int d^3r \ n_\uparrow(r) n_\downarrow(r). \quad (12)$$

The dependence of the critical temperature on the density ratio  $n_h/n_I$  and  $U$  is shown in Fig. 4. As expected, stronger on-site interactions strengthen the ferromagnetism and increase the Curie temperature. It is also natural to see that on-site interactions suppress quantum frustrations and the critical temperature becomes more mean-field like. Finally, we would like to emphasize that the self-consistent Green's function approach combines the mean-field and spin-wave theories and gives a complete description of DMS at finite temperature.

We thank Sankar Das Sarma and Allan MacDonald for fruitful discussions. HHL appreciates financial support from the National Science Council in Taiwan through the Ta-You Wu Fellowship and grants NSC-93-2120-M-007-005 and NSC-94-2112-M-007-031. The hospitality of KITP, where part of the work was carried out, and support from NSF PHY99-07949 are great appreciated.

---

- [1] H. Ohno, *Science* **281**, 951 (1998).
- [2] S. A. Wolf *et al.*, *Science* **294**, 1488 (2001).
- [3] H. Akai, *Phys. Rev. Lett.* **81**, 3002 (1998).
- [4] T. Dietl, H. Ohno, F. Matsukura, J. Cibert and D. Ferrand, *Science* **287**, 1019 (2000).
- [5] J. König, H.-H. Lin, and A. H. MacDonald, *Phys. Rev. Lett.* **84**, 5628 (2000).
- [6] J. Schliemann, J. König, H.-H. Lin and A. H. MacDonald, *Appl. Phys. Lett.* **78**, 1550 (2001).
- [7] V. I. Litvinov and V. K. Dugaev, *Phys. Rev. Lett.* **86**, 5593 (2001).
- [8] M. Berciu and R. N. Bhatt, *Phys. Rev. Lett.* **87**, 107203 (2001); *Phys. Rev. B* **69**, 045202 (2004).
- [9] D. J. Priour, Jr. E. H. Hwang and S. Das Sarma, *Phys. Rev. Lett.* **92**, 117201 (2004).
- [10] Note that the inclusion of a realistic band structure is crucially important for a *quantitative* description but does not change the physical picture *qualitatively*.
- [11] Herbert B. Callen, *Phys. Rev.* **130**, 890 (1963).
- [12] J. Schliemann, J. König and A. H. MacDonald, *Phys. Rev. B* **64**, 165201 (2001).

- [13] K. W. Edmonds, *et al.*, Phys. Rev. Lett. **92**, 037201 (2004).
- [14] H. Ohno, J. Magn. Magn. Mater. **200**, 110 (1999).
- [15] For a recent review, see A. H. MacDonald, P. Schiffer and N. Samarth, Nat. Mat. **4**, 195 (2005).